SAR Moving Target Imaging in a Sparsity-driven Framework

N. Özben Önhon and Müjdat Çetin

Faculty of Engineering and Natural Sciences, Sabancı University, Orhanlı, Tuzla, 34956 Istanbul, Turkey

ABSTRACT

In synthetic aperture radar (SAR) imaging, sparsity-driven imaging techniques have been shown to provide high resolution images with reduced sidelobes and reduced speckle, by allowing the incorporation of prior information about the scene into the problem. Just like many common SAR imaging methods, these techniques also assume the targets in the scene are stationary over the data collection interval. Here, we consider the problem of imaging in the presence of targets with unknown motion in the scene. Moving targets cause phase errors in the SAR data and these errors lead to defocusing in the corresponding spatial region in the reconstructed image. We view phase errors resulting from target motion as errors on the observation model of a static scene. Based on these observations we propose a method which not only benefits from the advantages of sparsity-driven imaging but also compansates the errors arising due to the moving targets. Considering that in SAR imaging the underlying scene usually admits a sparse representation, a nonquadratic regularization-based framework is used. The proposed method is based on minimization of a cost function which involves regularization terms imposing sparsity on the reflectivity field to be imaged, as well as on the spatial structure of the motion-related phase errors, reflecting the assumption that only a small percentage of the entire scene contains moving targets. Experimental results demonstrate the effectiveness of the proposed approach in reconstructing focused images of scenes containing multiple targets with unknown motion.

Keywords: SAR imaging, phase errors, regularization-based image reconstruction, sparse signal representation, moving target imaging

1. INTRODUCTION

Regularization-based image reconstruction has succesfully been applied to SAR imaging and it is shown that it has many advantages over conventional imaging.[1] These techniques can alleviate the problems in the case of incomplete data or sparse apertures. Moreover, they produce images with increased resolution, reduced sidelobes, and reduced speckle by incorporation of prior information about the features of interest and imposing various constraints (e.g., sparsity, smoothness) about the scene. Such algorithms assume that the mathematical model of the imaging system is perfectly known. However, in practice, it is very common to encounter various types of model errors. In synthetic aperture radar (SAR) imaging one predominant example of model errors is phase errors. Uncertainties on the position of the sensing platform or on the motion of the targets in the underlying scene cause phase errors in the SAR data and subsequently defocusing in the reconstructed image. Phase errors arising due to uncertainties in the position of the SAR sensing platform cause space-invariant defocusing, i.e., the amount of the defocusing in the reconstructed image is the same for all points in the scene. However, moving targets in the scene induce a space-variant defocus, i.e., defocusing appears only around the positions of the moving targets whereas the stationary background is not defocused.[2]

Motivated by these observations and considering that in the context of SAR imaging of man-made objects, the underlying scene, dominated by strong metallic scatterers, usually exhibits a sparse structure,

Further author information:
N. Özben Önhon: E-mail: onhon@sabanciuniv.edu
Müjdat Çetin : E-mail: mcetin@sabanciuniv.edu

we previously proposed a sparsity-driven technique for joint SAR imaging and space-invariant focusing by using a nonquadratic regularization-based framework.[3,4] Here, we present an extension of this framework for the *space-variant* defocusing problem. In this technique, the problem is handled as an optimization problem, in which besides the constraint on the sparsity of the reflectivity field, also a constraint on the spatial sparsity of the phase errors is imposed based on the assumption that motion in the scene is limited to a small number of spatial locations. The method is performed through iterative minimization of a cost function of both the field and the phase errors. Each iteration consists of two steps, the first of which is for image formation and the second is for phase error estimation. For phase error estimation we present two approaches. The first approach looks for potential motion and estimates the phase errors at all points in the scene. The second approach aims to improve the computational efficiency of the phase error estimation procedure by first determining regions of interest for potential motion using a fast procedure, and then performing phase error estimation only in these regions. Experimental results on various synthetic scenes demonstrate the effectiveness of the proposed method.

2. SAR IMAGING MODEL

In most SAR applications, the transmitted signal is a chirp signal, which has the following form:

$$s(t) = Re\left\{e^{j(\omega_0 t+\alpha t^2)}\right\} \tag{1}$$

Here, ω_0 is the center frequency and 2α is the so-called chirp-rate. The received signal $q_m(t)$ at the $m-th$ aperture position with a corresponding look angle of θ involves the convolution of the transmitted chirp signal with the projection $p_m(u)$ of the field at that observation angle.

$$q_m(t) = Re\left\{\int p_m(u)e^{j[\omega_0(t-\tau_0-\tau(u))+\alpha(t-\tau_0-\tau(u))^2]}du\right\} \tag{2}$$

Here, τ_0 represents the time required for the transmitted signal to propagate to the scene center and back. $\tau_0+\tau(u)$ is the delay for the returned signal from the scatterer at the range of d_0+u, where d_0 is the distance between the SAR sensor and the scene center. The data used for imaging are obtained after a pre-processing operation involving mixing and filtering steps.[5] After this process, the relation between the field $F(x,y)$ and the pre-processed SAR data $r_m(t)$ becomes

$$r_m(t) = \iint\limits_{x^2+y^2\leq L^2} F(x,y)e^{-jU(x\cos\theta+y\sin\theta)}dxdy \tag{3}$$

where

$$U = \frac{2}{c}(\omega_0 + 2\alpha(t-\tau_0)) \tag{4}$$

and L is the radius of the illuminated area. All of the returned signals from all observation angles constitute a patch from the two dimensional spatial Fourier transform of the corresponding field. The corresponding discrete model including all returned signals is as follows.

$$\underbrace{\begin{bmatrix} r_1 \\ r_2 \\ \\ \\ r_M \end{bmatrix}}_{r} = \underbrace{\begin{bmatrix} C_1 \\ C_2 \\ \\ \\ C_M \end{bmatrix}}_{C} f \tag{5}$$

Here, r_m is the vector of observed samples, C_m is a discretized approximation to the continuous observation kernel at the $m-th$ aperture position, f is a vector representing the unknown sampled reflectivity image

and M is the total number of aperture positions. The vector r is the SAR phase history data of all points in the scene. It is also possible to view r as the sum of the SAR data corresponding to each point in the scene.

$$r = \underbrace{C_{clmn-1} f(1)}_{rp_1} + \underbrace{C_{clmn-2} f(2)}_{rp_2} + .. + .. + \underbrace{C_{clmn-I} f(I)}_{rp_I} \tag{6}$$

Here, C_{clmn-i} is the $i-th$ column of the model matrix C and, $f(i)$ and rp_i represent the complex reflectivity at the $i-th$ point of the scene and the corresponding SAR data, respectively. I is the total number of points in the scene. The cross-range component of the target velocity causes the image of the target to be defocused in the cross-range direction, whereas the range component causes shifting in the cross-range direction and defocusing in both cross-range and range directions.[6,7] The image of a target that experiences significant vibration is defocused in the cross-range direction as well.[8] The defocusing arises due to the phase errors in the SAR data of these targets. Let us view the $i-th$ point in the scene as a point target having a motion which results in defocusing along the cross-range direction. The SAR data of this target can be expressed as:[6,7]

$$\begin{bmatrix} rp_{i_{1_e}} \\ rp_{i_{2_e}} \\ . \\ . \\ . \\ rp_{i_{M_e}} \end{bmatrix} = \begin{bmatrix} e^{j\phi_i(1)}\ rp_{i_1} \\ e^{j\phi_i(2)}\ rp_{i_2} \\ . \\ . \\ . \\ e^{j\phi_i(M)}\ rp_{i_M} \end{bmatrix} \tag{7}$$

Here, ϕ_i represents the phase error caused by the motion of the target and, rp_i and rp_{i_e} are the phase history data for the stationary and moving point target, respectively. In a similar way, this relation can be expressed in terms of the model matrix C as follows:

$$\begin{bmatrix} C_{clmn-i_1}(\phi) \\ C_{clmn-i_2}(\phi) \\ . \\ . \\ . \\ C_{clmn-i_M}(\phi) \end{bmatrix} = \begin{bmatrix} e^{j\phi_i(1)}\ C_{clmn-i_1} \\ e^{j\phi_i(2)}\ C_{clmn-i_2} \\ . \\ . \\ . \\ e^{j\phi_i(M)}\ C_{clmn-i_M} \end{bmatrix} \tag{8}$$

Here, $C_{clmn-i}(\phi)$ is the i-th column of the model matrix $C(\phi)$ that takes the movement of the targets into account and $C_{clmn-i_m}(\phi)$ is the part of $C_{clmn-i}(\phi)$ for the $m-th$ cross-range position. In the presence of additional observation noise, the observation model for the overall system becomes

$$g = C(\phi) f + v \tag{9}$$

where, v is the observation noise. Here, the aim is to estimate f and ϕ from the noisy observation g.

3. PROPOSED METHOD

We propose a sparsity-driven method for joint estimation of the field and phase errors caused by the moving targets which result in defocusing in cross-range direction. The method is based on a nonquadratic regularization-based framework which allows the incorporation of the prior sparsity information about the field and about the phase errors into the problem. The phase errors are incorporated into the problem using the vector β, which includes phase errors corresponding to all points in the scene, for all aperture positions.

$$\beta = \begin{bmatrix} \beta_1 \\ \beta_2 \\ . \\ . \\ . \\ \beta_M \end{bmatrix} \tag{10}$$

Here, β_m is the vector of phase errors for the $m-th$ aperture position and has the following form:

$$\beta_m = \left[e^{j\phi_1(m)}, e^{j\phi_2(m)}, ..., e^{j\phi_I(m)}\right]^T \tag{11}$$

The method is performed by minimizing the following cost function with respect to the field and phase errors.

$$\arg\min_{f,\beta} J(f,\beta) = \arg\min_{f,\beta} \|g - C(\phi)f\|_2^2 + \lambda_1 \|f\|_1 + \lambda_2 \|\beta - \mathbf{1}\|_1$$
$$s.t. \quad |\beta(i)| = 1 \quad \forall i \tag{12}$$

Here, $\mathbf{1}$ is a $MI \times 1$ vector of ones. Since the number of moving points is much less than the total number of points in the scene, most of the ϕ values in the vector β are zero. Since the elements of β are in the form of $e^{j\phi}$'s, when ϕ is zero, β becomes one. Therefore, this sparsity on the phase errors is incorporated into the problem by using the regularization term $\|\beta - \mathbf{1}\|_1$.

This problem is solved similarly to the optimization problem in a previous work on SAR imaging.[9] The algorithm is iterative and at each iteration, in first step, the cost function $J(f,\beta)$ is minimized with respect to the field f.

$$\hat{f}^{(n+1)} = \arg\min_f J(f, \hat{\beta}^{(n)}) = \arg\min_f \left\|g - C^{(n)}(\phi)f\right\|_2^2 + \lambda_1 \|f\|_1 \tag{13}$$

This minimization problem is solved using a previously proposed technique.[1] In the second step of each iteration, we use the field estimate $\hat{f}$ from the first step and estimate the phase errors by minimizing the following cost function for each aperture position:

$$\hat{\beta}_m^{(n+1)} = \arg\min_{\beta_m} J(\hat{f}^{(n+1)}, \beta_m) = \arg\min_{\beta_m} \left\|g_m - C_m T^{(n+1)} \beta_m\right\|_2^2 + \lambda_2 \|\beta_m - \mathbf{1}\|_1$$
$$s.t. \quad |\beta_m(i)| = 1 \quad \forall i \tag{14}$$

Here, T is a diagonal matrix, with the entries $\hat{f}(i)$ on its main diagonal, as follows:

$$T^{(n+1)} = diag\left\{\hat{f}^{(n+1)}(i)\right\} \tag{15}$$

In (14), $\mathbf{1}$ is a $I \times 1$ vector of ones. The constrained optimization problem in (14) is replaced with the following unconstrained problem that incorporates a penalty term on the magnitudes of $\beta_m(i)$'s.

$$\hat{\beta}_m^{(n+1)} = \arg\min_{\beta_m} \left\|g_m - C_m T^{(n+1)} \beta_m\right\|_2^2 + \lambda_2 \|\beta_m - \mathbf{1}\|_1 + \lambda_3 \sum_{i=1}^{I} (|\beta_m(i)| - 1)^2$$
$$= \arg\min_{\beta_m} \left\|g_m - C_m T^{(n+1)} \beta_m\right\|_2^2 + \lambda_2 \|\beta_m - \mathbf{1}\|_1 + \lambda_3 \|\beta_m\|_2^2 - 2\lambda_3 \|\beta_m\|_1$$
$$m = 1, 2, ..., M \tag{16}$$

This optimization problem is solved by using the same technique as in the field estimation step. Using the estimate $\hat{\beta}_m$, the following matrix is created,

$$B_m^{(n+1)} = diag\left\{\hat{\beta}_m^{(n+1)}(i)\right\} \tag{17}$$

which is used to update the model matrix for the $m-th$ aperture position.

$$C_m^{(n+1)}(\phi) = C_m B_m^{(n+1)} \tag{18}$$

After these phase estimation and model matrix update procedures have been completed for all aperture positions, the algorithm passes to the next iteration, by incrementing n and returning to (13).

3.1 Phase Error Estimation and Correction by Determining Regions of Interest (ROI)

The approach we have described in the previous section looks for potential motion everywhere in the scene. However, moving points usually exist in limited regions of a scene. Let us consider a scene containing a few moving vehicles. In this case, only a small portion of the entire scene will contain motion, and all the points belonging to a vehicle will have the same motion. In order to exploit such a structure both for computational gains and for improved robustness, we present a modified phase error estimation procedure. In the phase error estimation step of every iteration to solve the optimization problem in (12), we use a two-level approach. In the first level, we determine the range lines that are likely to contain moving objects. This generates regions of interest which we use in the second level to estimate the phase error. Assuming that the targets in each of these regions have the same motion and clutter is not strong, we perform space-invariant phase error estimation and compensation for each region. Now let us describe the overall phase error estimation step in detail. In the first level of the phase error estimation step the following cost function is minimized with respect to phase errors.

$$\hat{\beta}_m^{(n+1)} = \arg\min_{\beta_m} J(\hat{f}^{(n+1)}, \beta_m) = \arg\min_{\beta_m} \left\| g_m - C_m T^{(n+1)} \beta_m \right\|_2^2 + \lambda_2 \left\| \beta_m - \mathbf{1} \right\|_1 \tag{19}$$

Note that this optimization problem is slightly different from the one in (14) in the sense that the constraint on the magnitudes of the vector β is missing. This slight modification leads to significant computational savings. Since the goal of this first level is just to determine the ROI, rather than estimating β perfectly, the inaccuracies caused by this modification do not have a significant impact on overall performance. Then a matrix P is created, columns of which are the phase values of the β_m vectors.

$$P = \left[\begin{array}{cccc} \angle\beta_1 & \angle\beta_2 & \dots & \angle\beta_M \end{array} \right] \tag{20}$$

i-th row of the matrix P corresponds to the phase error vector for the i-th point in the scene. After taking the absolute value of each element of the matrix P, an $I \times 1$ vector P_{sum} is created by summing the elements in each row.

$$P_{sum}(i) = \sum_{m=1}^{M} abs\left(P\left(i,m\right)\right) \quad \forall i \tag{21}$$

Let the total number of image domain range indices be J and the total number of image domain cross-range indices be S. By reshaping the vector P_{sum} to an $S \times J$ matrix and then summing the elements in each column of this matrix, a $1 \times J$ vector V is obtained which includes a phase error-related value for each range line in the scene. For the range lines in which moving targets exist, this value is relatively greater than the values for other range lines. The vector V is normalized and the range lines having a value greater than 0.3 are decided to be range lines that potentially contain moving targets. This completes the first level of the phase error estimation step. The second level involves estimation of the phase error in each region determined in the first level. We assume that adjacent range lines correspond to the same target and apply space-invariant focusing for each spatially distinct region. This reduces the number of unknown phase error terms as compared to our more generic approach described at the beginning of Section 3, and leads to improved robustness in cases where the assumption that there is a single motion in each spatially connected ROI is valid. To simply explain the second level of the phase error estimation procedure, let us assume that there is only one moving target in the scene. Let the parts of the model matrix and the field corresponding to the region of interest be C_{reg} and f_{reg}, and the parts of model matrix and the field corresponding to the outside of this region be C_{out} and f_{out}, respectively. Then the phase error ϕ_{reg} is estimated by minimizing the following cost function for every aperture position

$$\hat{\phi}_{reg}^{(n+1)}(m) = \arg\min_{\phi_{reg}(m)} \left\| g_{reg_m}^{(n+1)} - e^{j\phi_{reg}(m)} C_{reg_m} \hat{f}_{reg}^{(n+1)} \right\|_2^2 \tag{22}$$
$$for\ m = 1, 2, ..., M$$

where g_{reg} is the phase history data corresponding to the region of interest and is given by:

$$g_{reg}^{(n+1)} = g - C_{out}\hat{f}_{out}^{(n+1)} \tag{23}$$

The problem in (22) is solved in closed form for every aperture position.[3,4] Using the phase error estimate, the corresponding part of the model matrix is updated.

$$C_{reg_m}(\hat{\phi}_{reg}^{(n+1)}(m)) = e^{j\hat{\phi}_{reg}^{(n+1)}(m)}C_{reg_m} \quad for \;\; m = 1, ..., M \tag{24}$$

If there are more than one moving targets in the scene, then this procedure is implemented for all regions with a potentially moving target. After the model matrix has been updated, the algorithm passes to the next iteration, by incrementing n and returning to the field estimation step.

4. EXPERIMENTAL RESULTS

We present experimental results on three different synthetic scenes. The scene for the first experiment is shown in Figure 1(a). There are four targets in the scene one of which (the leftmost one) is stationary and the other three have different motions. To simulate different motions and velocities of the targets, the phase history data of each target are corrupted by a different phase error function. The phase histories of the two targets lying in the right side of the scene are corrupted by independent random phase error functions uniformly distributed in $[-\pi/2, \pi/2]$ to simulate a vibration effect. The phase history data of the remaining target, third one from right in the scene, are corrupted by a quadratic phase error function to simulate a constant motion in cross-range direction. In Figure 1, the results of this experiment are displayed. In the results for conventional imaging and sparsity-driven imaging without any phase error correction, the defocusing and artifacts in the reconstructed images caused by the moving targets are clearly seen. On the other hand, images reconstructed by the proposed method are well focused and exhibit the advantages of sparsity-driven imaging such as high resolution, reduced speckle and sidelobes. In the second experiment, the scene involves many stationary point targets and two moving targets with constant velocities of $5m/s$ and $8m/s$ in the cross-range direction. The SAR system parameters for this experiment are shown in Table 1. For the two moving targets the cross-range velocity induced quadratic phase error is computed as follows:[7]

Table 1. SAR System Parameters

range resolution ρ_r	$1m$
cross-range resolution ρ_{cr}	$1m$
wavelength λ	$0.02m$
angular range $(\Delta\theta)$	0.573^o
center frequency f_0	$15GHz.$
distance between the SAR platform and patch center d_0	$30000m$
platform velocity v_p	$300m/s$
aperture time $T = \frac{\lambda d_0}{2v_p\rho_{cr}}$	$1s$

$$\phi(t) = \frac{4\pi v_{cr} v_p t_s^2}{\lambda d_0} \tag{25}$$

Here, t_s is the slow-time variable (continuous variable along the cross-range) and v_{cr} is the constant cross-range velocity of the target. According to this relationship, the target with velocity $5m/s$ and the target with velocity $8m/s$ will induce a quadratic phase error defined over an aperture $-T/2 \leq t_s \leq T/2$ with a center to edge amplitude of 2.5π radians and 4π radians, respectively. In Figure 2, the results for this experiment

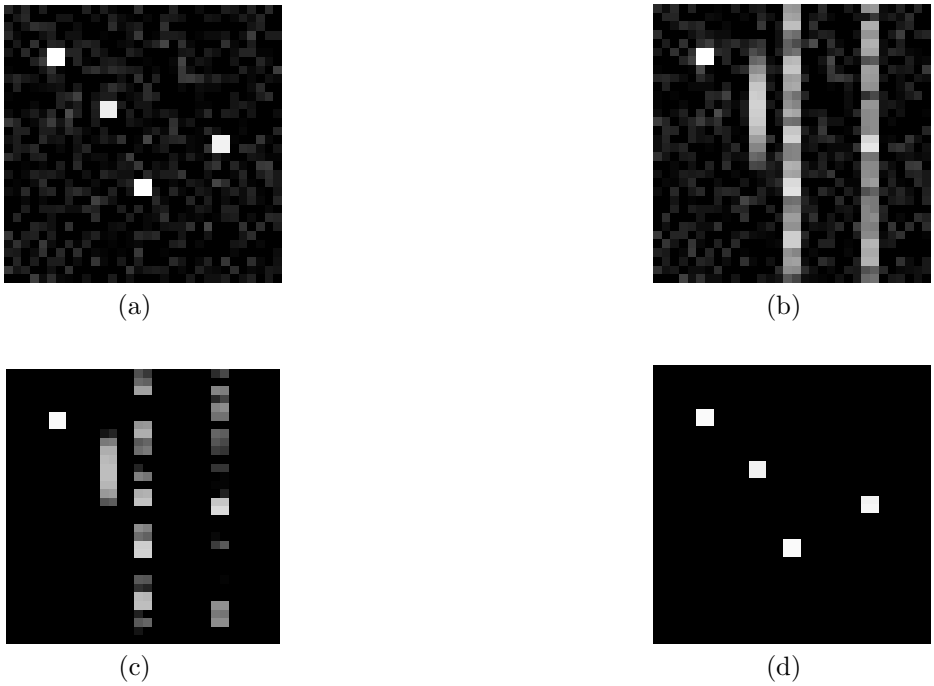

Figure 1. a) Original scene. b) Image reconstructed by conventional imaging. c) Image reconstructed by sparsity-driven imaging. d) Image reconstructed by the proposed method.

are displayed. In this experiment, we present the results of our general approach as well as our ROI-based approach. As shown in Figure 2, the two approaches produce successful and visually indistinguishable results. In the third experiment, performed on another synthetic scene involving many point-like targets and a larger rigid-body target, the SAR system parameters displayed in Table 1 are used. The phase history data of the rigid-body target are corrupted with a quadratic phase error of a center to edge amplitude of 4π radians which corresponds to a cross-range velocity of $8m/s$. In this experiment, we employ our ROI-based approach. The result shows the effectiveness of the approach in estimating and compensating phase errors.

5. CONCLUSION

In this work we have presented a sparsity-driven method for joint imaging and space-variant focusing in SAR. The method effectively produces high resolution images and removes the phase errors causing defocusing in the cross-range direction. On various synthetic scenes we have presented experimental results which show the effectiveness of our approach. Our planned future work involves application of the proposed method on real SAR data. With some extensions, the method can be used to compansate phase errors imposed by targets with a motion in range direction, as well.

ACKNOWLEDGMENTS

This work was partially supported by the Scientific and Technological Research Council of Turkey under Grant 105E090, and by a Turkish Academy of Sciences Distinguished Young Scientist Award.

REFERENCES

1. M. Çetin and W.C. Karl, "Feature-enhanced synthetic aperture radar image formation based on non-quadratic regularization," *IEEE Trans. Image Processing*, vol. 10, no. 4, pp. 623–631, 2001.

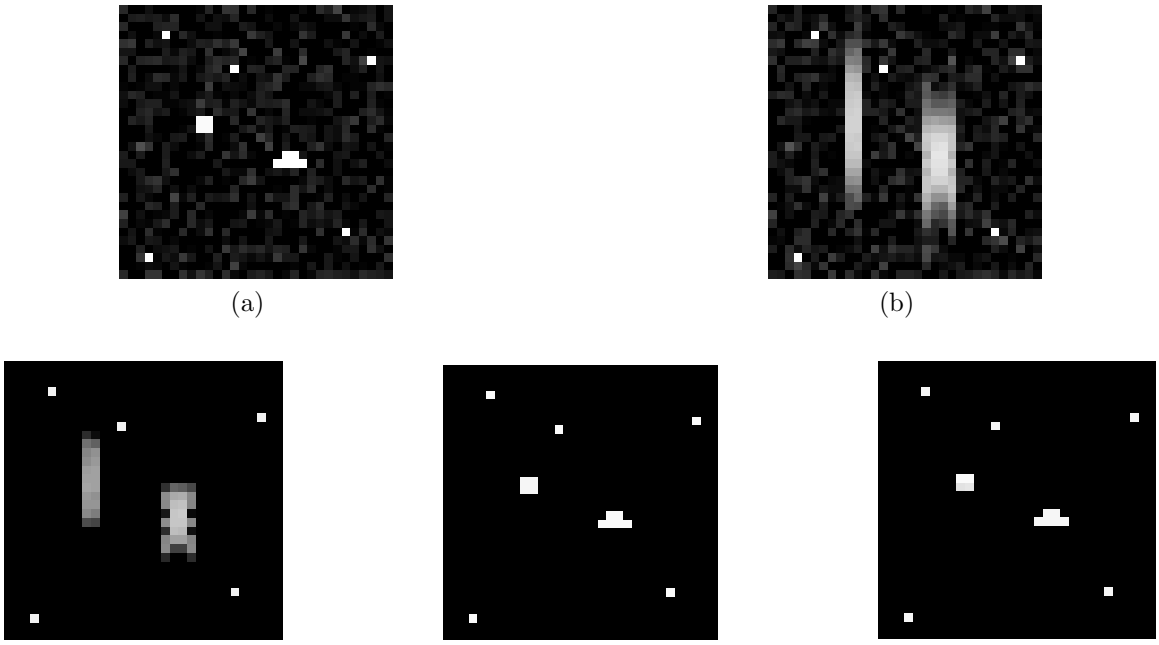

Figure 2. a) Original scene. b) Image reconstructed by conventional imaging. c) Image reconstructed by sparsity-driven imaging. d) Image reconstructed by the proposed method. e) Image reconstructed by the proposed method with phase error estimation for ROI.

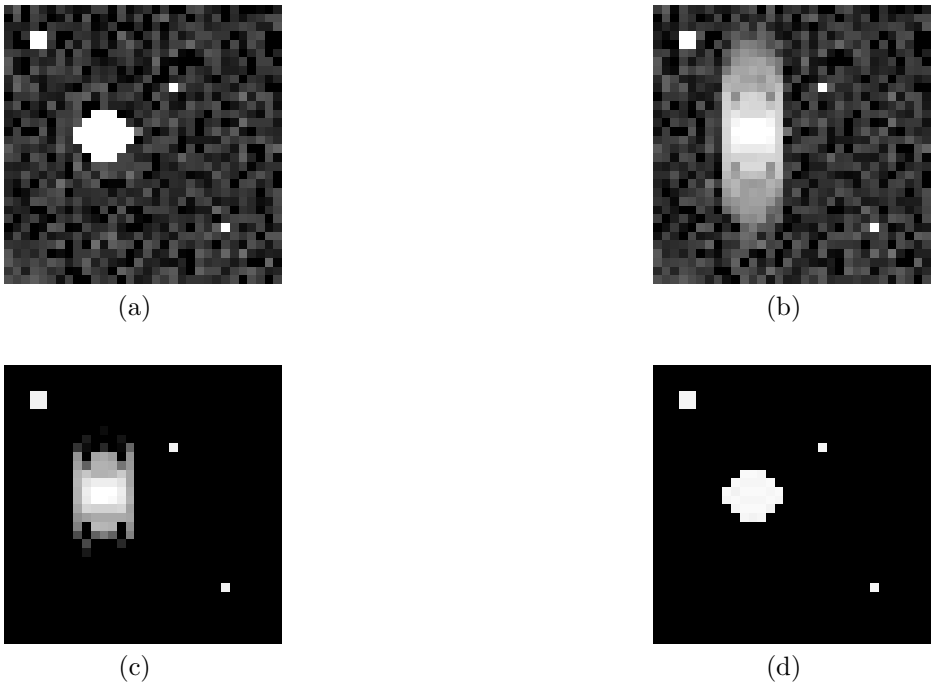

Figure 3. a) Original scene. b) Image reconstructed by conventional imaging. c) Image reconstructed by sparsity-driven imaging. d) Image reconstructed by the proposed method with phase error estimation for ROI.

2. W. G. Carrara, R. M. Majewski, and R. S. Goodman, *Spotlight Synthetic Aperture Radar: Signal Processing Algorithms*, Artech House, 1995.
3. N. Ö. Önhon and M. Çetin, "A nonquadratic regularization based technique for joint SAR imaging and model error correction," *Algorithms for Synthetic Aperture Radar Imagery XVI, Proc. SPIE*, vol. 7337, 2009.
4. N. Ö. Önhon and M. Çetin, "Joint sparsity-driven inversion and model error correction for radar imaging," *IEEE Int. Conf. Acoustics, Speech, Signal Processing*, pp. 1206–1209, 2010.
5. C. V. Jakowatz, Jr., D. E. Wahl, P. H. Eichel, D. C. Ghiglia, and P. A. Thompson, *Spotlight-Mode Synthetic Aperture Radar: A Signal Processing Approach*, Springer, 1996.
6. C. V. Jakowatz, Jr., D. E. Wahl, and P. H. Eichel, "Refocus of constant velocity moving targets in synthetic aperture radar imagery," *Algorithms for Synthetic Aperture Radar Imagery V, SPIE*, 1998.
7. J. R. Fienup, "Detecting moving targets in SAR imagery by focusing," *IEEE Transactions on Aerospace and Electronic Systems*, vol. 37, no. 3, pp. 794–809, 2001.
8. A. R. Fasih, B. D. Rigling, and R. L. Moses, "Analysis of target rotation and translation in SAR imagery," *Algorithms for Synthetic Aperture Radar Imagery XVI, SPIE*, 2009.
9. S. Samadi, M. Çetin, and M. A. Masnadi-Shirazi, "Sparse representation-based synthetic aperture radar imaging," *IET Radar, Sonar and Navigation*, vol. 5, no. 2, pp. 182–193, 2011.